



Available online at www.sciencedirect.com

ScienceDirect

Comput. Methods Appl. Mech. Engrg. 280 (2014) 117–134

**Computer methods
in applied
mechanics and
engineering**

www.elsevier.com/locate/cma

A reduced multiscale model for nonlinear structural topology optimization

Liang Xia*, Piotr Breitkopf

Laboratoire Roberval, UMR 7337 UTC-CNRS, Université de Technologie de Compiègne, Centre de Recherches de Royallieu, CS 60319, 60203, Compiègne Cedex, France

Received 9 October 2013; received in revised form 3 March 2014; accepted 23 July 2014

Available online 1 August 2014

Abstract

This paper presents a reduced multiscale model for macroscopic structural design considering microscopic material nonlinear microstructures. This work introduces Reduced Order Model (ROM) to alleviate the heavy computational demand of nonlinear nested multiscale procedures, particularly in an optimization framework which requires multiple loops involving similar computations. The surrogate model constructed using Proper Orthogonal Decomposition (POD) and Diffuse Approximation reduces the computational effort for solving the microscopic boundary value problems. Multiscale analysis model (FE^2) is applied to link structure and microstructures in the two scales. Maximum stiffness design of the macroscopic structure is realized using a discrete level-set topology optimization model. It is shown by means of numerical tests that the reduced multiscale model provides reasonable designs as compared to those obtained by the unreduced model while with a significantly reduced computational effort.

© 2014 Elsevier B.V. All rights reserved.

Keywords: Model reduction; Proper Orthogonal Decomposition; Diffuse Approximation; Multiscale analysis; Parallel computing; Topology optimization

1. Introduction

The constant increase of computing capabilities enables computational investigation of materials at the microscopic level. At the same time, the fast progress made in the field of material science allows us to control the material microstructure composition to an unprecedented extent [1]. Therefore, there is an increasing research demand of simultaneous material and structural designs in the framework of multiscale analysis.

The most representative field of numerical material researches is homogenization which pursues to depict material macroscopic constitutive behavior using the homogenized values of a chosen Representative Volume Element (RVE). However, such approach encounters difficulties in dealing with geometrical and physical nonlinearities. Multiscale incremental homogenization approaches have been proposed [2–8] and largely developed in the last decade [9] in order to assess the macroscopic influence of microscopic heterogeneities. Generally speaking, this type of approach,

* Corresponding author. Tel.: +33 622770321.

E-mail address: liang.xia@utc.fr (L. Xia).

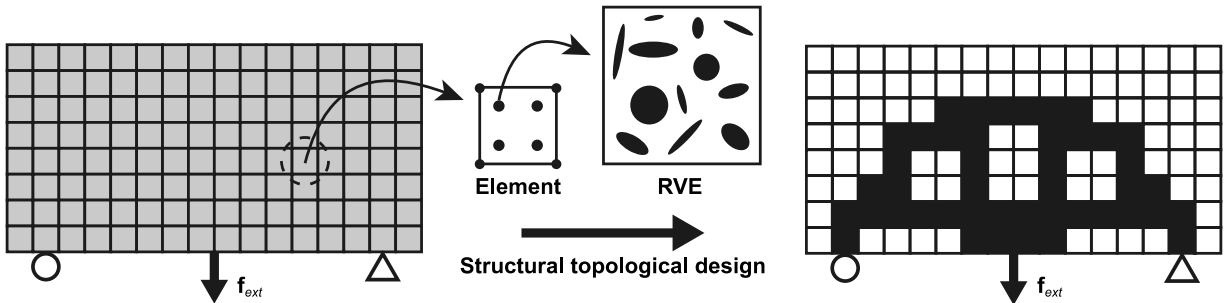


Fig. 1. Illustration of the considered multiscale structural optimization design.

or the so-called FE² [4], solves two nested boundary value problems, one at the macroscopic scale and another at the microscopic scale. The constitutive behavior at macroscopic integration points is determined using the averaged results of a detailed modeling of the microscopic RVE. The FE² approach is able to evaluate the macroscopic responses of heterogeneous material with an accurate account for micro characteristics and evolution of the morphology [5]. The challenges of the FE² approach are due to high computational effort, requiring parallel computing [4].

Alternatively, reduced order modeling has been systematically researched and widely used in the fields of computational mechanics in order to reduce computing time and data storage requirement [10,11]. Recently, several multidimensional reduction models have been proposed for material behavior, such as Proper Generalized Decomposition (PGD) [12], Hyper-reduction [13,14] and Nonuniform Transformation Field Analysis (NTFA) [15,16]. Some other applications can also be found for the representation of material microstructure [17,18] and structural optimization design [19,20]. The reduced model multiscale method (R3M) [21] applies an intrusive reduction approach to perform microscopic analysis on RVE in finite strain. The reduced basis of R3M is obtained using Proper Orthogonal Decomposition (POD) through off-line pre-computations. A significant gain in time has been observed and it has also been indicated by the authors themselves that in order to handle more severe nonlinearities or path-dependent problems, the reduced basis needs to be adapted in an on-line manner. PGD technique has been recently embedded into multiscale analysis, where [22] considered linear elasticity and applied PGD to parametrize microstructures at the micro scale and [23] considered nonlinear elasticity and proposed an improved version of PGD for the microscopic resolution.

From the aspect of structural design, topology optimization has become a promising approach in both academic researches and industrial applications [24]. Various models have been developed, such as density-based methods [25,26], evolutionary procedure [27], and level-set methods [28,29], to perform topology optimization in different manners. A critical review and comparison of the various models have been recently presented in [30]. Most structural topology optimization problems are restricted to the linear elastic regime. However, when material microscopic heterogeneities and nonlinear behaviors have to be taken into consideration in structural design, the multiscale analysis models have to be employed. [31] has recently presented a bi-level topology optimization in the framework of multiscale analysis, where both macroscopic and microscopic designs are performed using density-based topology optimization method involving parallel computing.

The central contribution of this paper is the introduction of Reduced Order Model (ROM) to perform multiscale topological optimization design (Fig. 1). The multiscale analysis model (FE²) [4] is applied to link the macroscopic structure and the corresponding RVE microstructures at the microscopic scale. The optimization process requires multiple design loops involving similar or even repeated computations of the RVE which perfectly suits the ROM learning process. In the present work the considered RVE is assumed to be the same for all macroscopic integration points. Maximum stiffness design of the macroscopic structure is performed using a discrete level-set topology optimization model [32]. The reduction is performed in an adaptive non-intrusive manner which is an alternative to the intrusive approach in [21]. The reduced basis is extracted using Proper Orthogonal Decomposition (POD) and the surrogate model is constructed using Diffuse Approximation [33], variant of Moving Least Squares [34].

The remainder of this paper is organized in the following manner: Section 2 briefly reviews the FE² approach which links the macroscopic structure and microscopic microstructure RVE; Section 3 presents the model for structural design using a discrete level-set model; Section 4 gives the bi-level reduced surrogate model which is constructed using POD and Diffuse Approximation; Section 5 showcases the model by several numerical test examples; the paper ends with concluding comments and suggestions for future work.

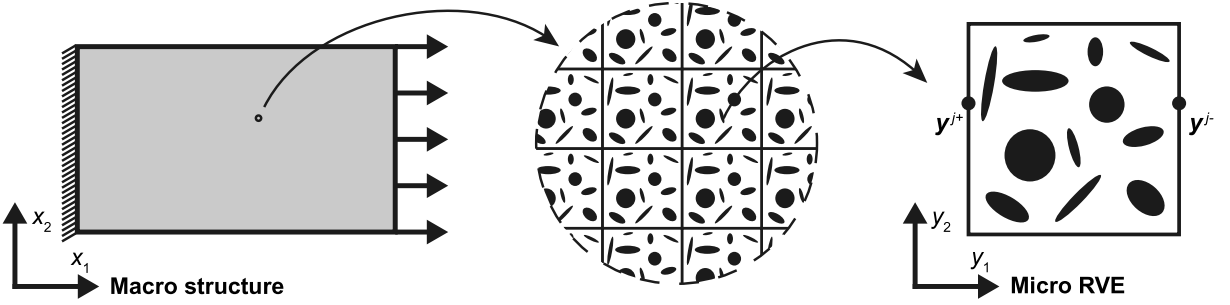


Fig. 2. Illustration of the selection of a typical 2D representative volume element (RVE).

2. FE² approach

The FE² approach [4] is chosen here to bridge the macroscopic structure and the corresponding microscopic RVE to serve structural topology optimization. The general principle and numerical implementations of this approach are introduced in the following.

2.1. General principle

The key hypothesis of FE² consists in the separation of macroscopic and microscopic scales. It is assumed that the microscopic length scale is large enough to be considered in the framework of continuum mechanics, and at the same time much smaller than the macroscopic length scale, such that RVE can be considered in terms of periodically ordered pattern [5], as illustrated in Fig. 2.

The principal concept of the FE² approach assumes that each macroscopic material point is attributed with a RVE so that the macroscopic stress and strain for the considered point can be estimated by averaging the corresponding stress and strain fields of the RVE. Thereafter, there is no need to specify the macroscopic constitutive behavior and we only need to define the constitutive behavior for each material phase of the RVE.

Let \mathbf{x} and \mathbf{y} denote the position of a point at the macroscopic and microscopic scales, respectively. At the macroscopic scale, stress and strain fields are denoted by $\Sigma(\mathbf{x})$ and $E(\mathbf{x})$, which are evaluated as the average of the corresponding microscopic fields $\sigma(\mathbf{x}, \mathbf{y})$ and $\epsilon(\mathbf{x}, \mathbf{y})$ over the RVE of region Ω_x corresponding to the material point \mathbf{x}

$$\begin{cases} \Sigma(\mathbf{x}) = \langle \sigma(\mathbf{x}, \mathbf{y}) \rangle = \frac{1}{|\Omega_x|} \int_{\Omega_x} \sigma(\mathbf{x}, \mathbf{y}) d\Omega_x \\ E(\mathbf{x}) = \langle \epsilon(\mathbf{x}, \mathbf{y}) \rangle = \frac{1}{|\Omega_x|} \int_{\Omega_x} \epsilon(\mathbf{x}, \mathbf{y}) d\Omega_x, \end{cases} \quad (1)$$

where $\langle \cdot \rangle$ denotes the average. The FE² performs the following steps:

- evaluate the macroscopic strain field $E(\mathbf{x})$ with an initially defined elastic tensor C_0 ;
- define periodic boundary conditions on the RVE at material point \mathbf{x} upon $E(\mathbf{x})$;
- evaluate the stress field $\sigma(\mathbf{x}, \mathbf{y})$ by solving boundary value problem of the RVE;
- compute the macroscopic stress tensor $\Sigma(\mathbf{x})$ at material point \mathbf{x} via averaging $\sigma(\mathbf{x}, \mathbf{y})$;
- update the structural displacement field $\mathbf{u}(\mathbf{x})$ using iterative Newton–Raphson method;
- repeat above procedures until the macroscopic force equilibrium is achieved.

2.2. Periodic homogenization analysis

The formulation of the periodic RVE can be derived in a systematic way using the two-scale asymptotic expansion method [35], or following a process which is also valid for random media [36], which is followed in this paper. Upon

the assumption of periodicity at the microscopic scale, the displacement field of the microstructure can be written as the sum of a macroscopic displacement field and a periodic fluctuation field \mathbf{u}^* [36]

$$\mathbf{u}(\mathbf{x}, \mathbf{y}) = \mathbf{E}(\mathbf{x}) \cdot \mathbf{y} + \mathbf{u}^*(\mathbf{y}). \quad (2)$$

Because $\mathbf{u}^*(\mathbf{y})$ is periodic, its strain average $\langle \boldsymbol{\epsilon}(\mathbf{u}^*) \rangle$ equals zero, and the average of microscopic strain thus equals directly to macroscopic strain

$$\langle \boldsymbol{\epsilon}(\mathbf{x}, \mathbf{y}) \rangle = \mathbf{E}(\mathbf{x}). \quad (3)$$

In order to compute microscopic stress field, the boundary value problem induced by an overall strain $\mathbf{E}(\mathbf{x})$ has to be solved at the microscopic scale on the RVE: find $\boldsymbol{\sigma}$, $\boldsymbol{\epsilon}$, \mathbf{u}^* such that

$$\begin{cases} \boldsymbol{\sigma}(\mathbf{x}, \mathbf{y}) = \mathbf{c}(\mathbf{y}) : (\mathbf{E}(\mathbf{x}) + \boldsymbol{\epsilon}(\mathbf{u}^*(\mathbf{y}))) \\ \operatorname{div} \boldsymbol{\sigma}(\mathbf{x}, \mathbf{y}) = 0, \mathbf{u}^* \text{ periodic}, \boldsymbol{\sigma} \cdot \mathbf{n} \text{ anti-periodic}, \end{cases} \quad (4)$$

where $\mathbf{c}(\mathbf{y})$ is the linear elastic tensor at the microscopic scale; “periodic” indicates that all components of \mathbf{u}^* take identical values on points of the opposite sides of the boundary $\partial\Omega_x$; “anti-periodic” indicates that all components of $\boldsymbol{\sigma} \cdot \mathbf{n}$ take opposite values on points of the opposite sides of $\partial\Omega_x$, deduced from the periodicity of $\boldsymbol{\sigma}$ and the fact that the normal vectors \mathbf{n} at the corresponding parallel sides of $\partial\Omega_x$ are opposite.

In practice, Eq. (2) cannot be directly applied to the boundaries since the periodic part \mathbf{u}^* is generally unknown. The general expression is usually transformed into a certain number of explicit constraints between the corresponding pairs of nodes on the opposite surfaces of the RVE [37]. Consider an RVE such as one periodic cellular microstructure in Fig. 2, the displacements on a pair of opposite boundaries are

$$\begin{cases} \mathbf{u}(\mathbf{x}, \mathbf{y})^{j+} = \mathbf{E}(\mathbf{x}) \cdot \mathbf{y}^{j+} + \mathbf{u}^*(\mathbf{y}) \\ \mathbf{u}(\mathbf{x}, \mathbf{y})^{j-} = \mathbf{E}(\mathbf{x}) \cdot \mathbf{y}^{j-} + \mathbf{u}^*(\mathbf{y}), \end{cases} \quad (5)$$

where superscripts “ $j+$ ” and “ $j-$ ” denote the pair of two opposite parallel RVE boundary surfaces that are oriented perpendicular to the j th direction. The periodic part \mathbf{u}^* can be eliminated through the difference between the displacements on the two opposite surfaces

$$\mathbf{u}^{j+} - \mathbf{u}^{j-} = \mathbf{E}(\mathbf{x}) \cdot (\mathbf{y}^{j+} - \mathbf{y}^{j-}), \quad (6)$$

in which the difference $\Delta\mathbf{y}_j = (\mathbf{y}^{j+} - \mathbf{y}^{j-})$ is constant for every pair of the parallel boundary surfaces. With specified $\mathbf{E}(\mathbf{x})$, the right side becomes constant and such equations can be easily be applied in the finite element analysis as nodal displacement constraint equations.

The application of Eq. (6) guarantees automatically the “periodic” condition of \mathbf{u}^* in Eq. (4). As for the “anti-periodic” condition of the tractions along the boundaries $\boldsymbol{\sigma} \cdot \mathbf{n}$ in Eq. (4), it has been proved in [38] that it can be also guaranteed by the application of Eq. (6) within the displacement-based finite element analysis framework. The average stress field can be evaluated as the ratio of resultant traction forces on the boundary surfaces to the corresponding areas of the boundary surfaces upon [37]

$$\langle \boldsymbol{\sigma} \rangle_{ij} = \frac{\Delta\mathbf{y}_j}{|V|} \int_{S_j} \boldsymbol{\sigma}_{ij} dS_j = \frac{(P_i)_j}{S_j}, \quad (\text{no summation over } j), \quad (7)$$

where S_j is the area of the boundary surface which is oriented perpendicular to the j th direction and $(P_i)_j$ is the resultant traction force acting in the i th direction on boundary surface S_j .

2.3. Finite element implementation of FE²

A schematic view of the FE² algorithm is depicted in Fig. 3, where each Gauss integration point is attributed with an RVE within the context of finite element analysis (FEA). In case of nonlinear elasticity, the displacement solution at the macroscopic scale is solved using the iterative Newton–Raphson method

$$\begin{cases} \mathbf{K}_T^{(k)} \Delta\mathbf{u}^{(k+1)} = \mathbf{f}_{ext} - \mathbf{f}_{int}^{(k)}(\mathbf{u}^{(k)}) \\ \mathbf{u}^{(k+1)} = \mathbf{u}^{(k)} + \Delta\mathbf{u}^{(k+1)}, \end{cases} \quad (8)$$

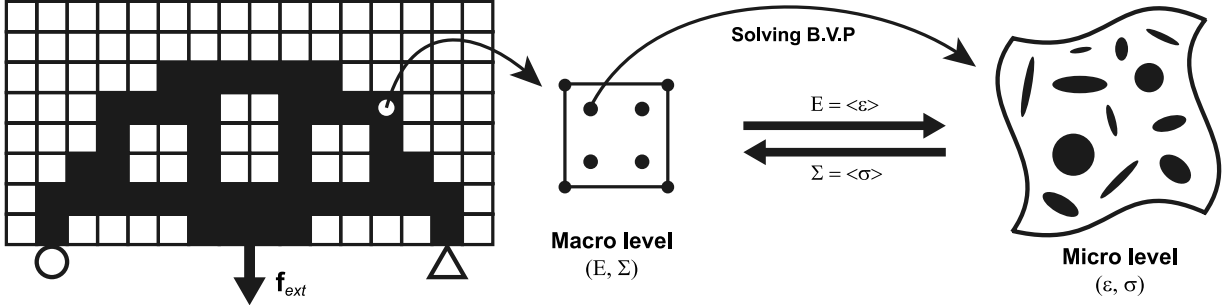


Fig. 3. Illustration of the implementation of FE^2 in the framework of FEA.

where $\mathbf{K}_T^{(k)}$ is the consistent tangent stiffness matrix at the k th iteration. However, when nonlinearity is involved at the microscopic scale, there exists no explicit closed-form expression of $\mathbf{K}_T^{(k)}$ at the macroscopic scale. One possible but time-consuming solution is to approximate this matrix using a perturbation method [4]. To be precise, the structural response is evaluated for a small strain variation $\delta\boldsymbol{\epsilon}$ at the converged substep solution. The $\mathbf{K}_T^{(k)}$ could be reconstructed by exciting each of the components of $\delta\boldsymbol{\epsilon}$. An alternative perturbation approach can be found in [5] based on nodal condensation.

It is worth noting that computing the tangent matrix by the perturbation method requires the finite element solutions of Eq. (4) four (in 2D) or six (in 3D) whose cost is not negligible. For this reason, [4,21] suggest to use initial stiffness matrix during the iteration process.

For a discretized macroscopic structure, the macroscopic strain is computed by

$$\mathbf{E}(\mathbf{x}) = \mathbf{B}^T(\mathbf{x})\mathbf{u}_e, \quad (9)$$

in which $\mathbf{B}(\mathbf{x})$ is the linear strain-displacement matrix of the considered Gauss point at \mathbf{x} , \mathbf{u}_e is the displacement vector of the considered element. After solving the boundary value problem of the RVE for the given prescribed overall strain load, the macroscopic stress $\boldsymbol{\Sigma}$ at each integration point can be evaluated via Eq. (7). Thereafter, the internal force \mathbf{f}_{int} in Eq. (8) can be evaluated based on the averaged stresses returned from the RVE level

$$\mathbf{f}_{int} = \int_{\Omega} \mathbf{B}^T \boldsymbol{\Sigma}(\mathbf{x}) d\Omega = \int_{\Omega} \mathbf{B}^T \langle \boldsymbol{\sigma}(\mathbf{x}, \mathbf{y}) \rangle d\Omega, \quad (10)$$

where Ω denotes the structural region defined at the macroscopic scale. The incremental procedure of Eq. (8) is repeated until the external and internal forces are in balance.

3. Nonlinear structural design using level-set method

Among all existing methods for topology optimization [30], we choose to use level-set method [28,29] to perform topology optimization design for the macroscopic structure. Note that unlike the homogenization method [25,26], the level-set method is not a relaxation method, which means that local optima have not been fully eliminated in favor of global optima [29]. Special attention needs to be paid here because in this work homogenization analysis is performed to link the two separated scales. Due to the fact that when the problem is solved numerically on a fixed Eulerian mesh, therefore intermediate material properties have to be attributed to the elements within the boundary region $\partial\Omega$, or the so-called “narrow-band” [28]. In order to avoid defining a pseudo-relationship between the intermediate values and the considered RVE, we choose to use the discrete version of level-set topology optimization model [32] to straightforwardly link RVEs to the solid region of the structure.

3.1. Discrete level-set model

An initial level-set function $\psi(x, t_0)$ is constructed as a signed distance function upon the discretized initial structural topology as shown in Fig. 4 following

$$\begin{cases} \psi(\mathbf{x}_e, t_0) < 0 & \text{if } \rho_e = 1 \\ \psi(\mathbf{x}_e, t_0) > 0 & \text{if } \rho_e = 0, \end{cases} \quad (11)$$

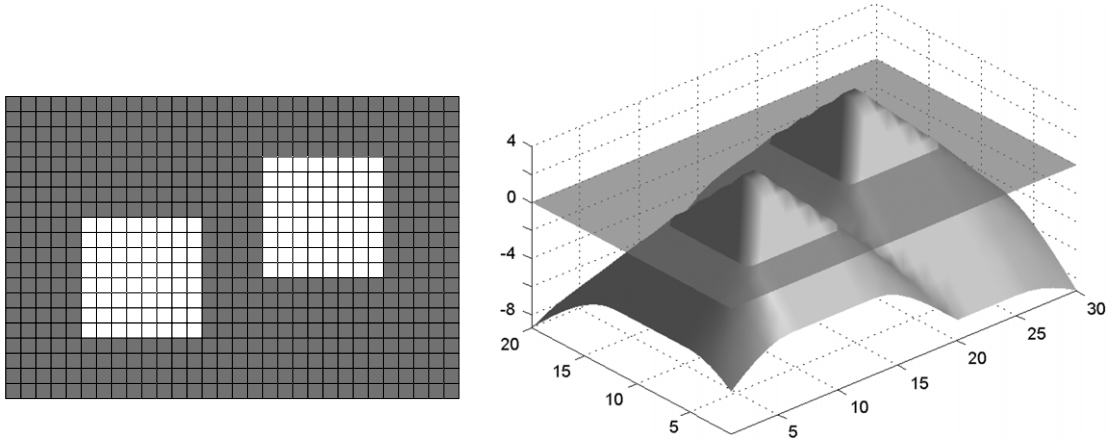


Fig. 4. A rectangular plate with two square holes and its discretized level-set function.

where \mathbf{x}_e denotes the center of the e th element and ρ_e is its pseudo-density. By constructing $\psi(\mathbf{x}_e, t_0) \neq 0$, $\rho_e = 1$ or 0 indicate element e is occupied by solid or void material correspondingly in sense of discrete topology optimization design, and no intermediate value is attributed to ρ_e . The initialized level-set function $\psi(x, t_0)$ is then be updated to $\psi(x, t)$ corresponding a new structural topology by solving the “Hamilton–Jacobi” evolution equation

$$\frac{\partial \psi(x, t)}{\partial t} + v_n |\nabla \psi(x, t)| = 0, \quad (12)$$

where t is a pseudo-time defined corresponding to different optimization iterations. The normal velocity field v_n determines geometric motion of the boundary of the structure and is chosen based on the shape derivative of the design objective. The updated level-set function $\psi(x, t)$ is then mapped to the discretized design domain through

$$\rho_e = \begin{cases} 1 & \text{if } \psi(\mathbf{x}_e, t) < 0 \\ 0 & \text{if } \psi(\mathbf{x}_e, t) > 0. \end{cases} \quad (13)$$

Note that, in practice in order to prevent the singularity of the stiffness matrix, a small value 10^{-4} is attributed to ρ_e to denote void elements.

It worth noting that the standard evolution equation of Eq. (12) cannot nucleate new void regions during the optimization process [29]. An additional forcing term based on the topological derivative of the design objective can be integrated into Eq. (12) to nucleate new holes within the structure [39]. In this work we follow the initial algorithm [28,29], for which a topology with “sufficient” holes is initially defined. The initial layout of holes is arbitrarily fixed. Though new holes cannot be nucleated, the initially defined holes can merge and split during the design, providing sufficient freedom for topological design or at least sufficient enough for the present work.

With above definitions, we have in fact introduced the concept of element pseudo-density in terms of level-set function $\rho(\psi)$ to perform the discretized topology optimization. At the macroscopic scale, material constitutive behavior is implicitly given in terms of the stress–strain relationship evaluated by the FE² scheme. The relationship between the macroscopic stress and the averaged microscopic stress of Gauss integration point \mathbf{x} of an element is defined in terms of ρ_e as

$$\Sigma(\mathbf{x}, \rho_e) = \rho_e \langle \sigma(\mathbf{x}, \mathbf{y}) \rangle, \quad (14)$$

where the microscopic stress field $\sigma(\mathbf{x}, \mathbf{y})$ is evaluated via the periodic homogenization analysis on the corresponding RVE with a prescribed overall strain

$$\mathbf{E}(\mathbf{x}) = \mathbf{B}^T(\mathbf{x}) \mathbf{u}_e, \quad (15)$$

in which $\mathbf{B}(\mathbf{x})$ is the linear strain–displacement matrix of the considered point \mathbf{x} within the element, \mathbf{u}_e is the displacement vector of the considered element.

3.2. Optimization model and sensitivity analysis

Within the context of multiscale analysis, the optimization objective corresponding to stiffness maximization or compliance minimization can be written in terms of $\rho(\psi)$

$$\begin{aligned} \min_{\rho(\psi)} : \quad & c(\rho(\psi)) = \mathbf{f}_{ext}^T \mathbf{u} \\ \text{s.t.} : \quad & \mathbf{R}(\mathbf{u}, \rho(\psi)) = \mathbf{0} \\ & V(\rho(\psi)) = \sum_{e=1}^N \rho_e = V_{req} \\ & \rho_e = 0 \text{ or } 1, \quad \forall e = 1, \dots, N, \end{aligned} \quad (16)$$

where $\rho = (\rho_1, \dots, \rho_N)$ is the vector of the element pseudo-densities. In the following, we will denote $\rho(\psi)$ by ρ to alleviate the notation. The objective $c(\rho)$ is twice of the strain energy. The macroscopic structural stiffness is maximized in terms of minimizing the global strain energy. $V(\rho)$ is the total number of solid elements and V_{req} is the required number of solid elements. \mathbf{u} is the final converged displacement solution. $\mathbf{R}(\mathbf{u}, \rho)$ stands for the force residual at the macroscopic scale

$$\mathbf{R}(\mathbf{u}, \rho) = \mathbf{f}_{ext} - \sum_{e=1}^N \int_{\Omega_e} \mathbf{B}^T \rho_e \langle \boldsymbol{\sigma}(\mathbf{x}, \mathbf{y}) \rangle d\Omega_e. \quad (17)$$

An augmented Lagrangian method is applied to convert the original constrained optimization problem Eq. (16) into an unconstrained problem as presented in [32,40,41]

$$L = c(\rho) + \lambda^k (V(\rho) - V_{req}) + \frac{1}{2\Lambda^k} (V(\rho) - V_{req})^2, \quad (18)$$

where λ^k is the Lagrangian multiplier and Λ^k is the penalty parameter updated iteratively with the optimization iteration k using the scheme [41]:

$$\lambda^{k+1} = \lambda^k + \frac{1}{\Lambda^k} (V(\rho) - V_{req}), \quad \Lambda^{k+1} = \alpha \Lambda^k, \quad (19)$$

where $\alpha \in (0, 1)$ is a parameter to be fixed by the user (see Section 5). The initial values of λ and Λ are decided according to the physical responses of the considered design problem [32,41].

In order to update the level-set function $\psi(x, t)$ and therefore the structural topology $\rho(\psi)$, the normal velocity v_n needs to be determined in Eq. (12). Conventionally, v_n is chosen as a descent direction for the Lagrangian L using its shape derivative [28,29]. The normal velocity v_n within an element e at design iteration k is derived as

$$v_n|_e = -\frac{\partial L}{\partial \rho_e} = -\frac{\partial c}{\partial \rho_e} - \lambda^k - \frac{1}{\Lambda^k} (V(\rho) - V_{req}), \quad (20)$$

where the partial derivative $\partial c / \partial \rho_e$ equals

$$\frac{\partial c}{\partial \rho_e} = \mathbf{f}_{ext}^T \frac{\partial \mathbf{u}}{\partial \rho_e}. \quad (21)$$

The determination of $\partial c / \partial \rho_e$ requires using the adjoint method.

Introducing a vector of Lagrangian multipliers \mathbf{w} , we have the objective $c(\rho)$ without changing the objective value, i.e., $c = c^*$:

$$c^*(\rho) = \mathbf{f}_{ext}^T \mathbf{u} + \mathbf{w}^T \mathbf{R}(\mathbf{u}, \rho), \quad (22)$$

where the term $\mathbf{w}^T \mathbf{R}(\mathbf{u}, \rho)$ equals zero when the macroscopic equilibrium of Eq. (17) is achieved. The sensitivity of the modified objective function with respect to ρ_e is

$$\frac{\partial c^*}{\partial \rho_e} = \mathbf{f}_{ext}^T \frac{\partial \mathbf{u}}{\partial \rho_e} + \mathbf{w}^T \left(\frac{\partial \mathbf{R}}{\partial \mathbf{u}} \frac{\partial \mathbf{u}}{\partial \rho_e} + \frac{\partial \mathbf{R}}{\partial \rho_e} \right), \quad (23)$$

Algorithm 1 The general optimization framework.

```

1: Initialize topology  $\rho_0$  and level-set  $\psi(x, t_0)$ ;
2: while  $\|\rho_{i+1} - \rho_i\| > \delta_{opt}$  { $i++$ } do
3:   loop over all macro time steps { $j++$ }
4:     while  $\|\mathbf{f}_{ext} - \mathbf{f}_{int}\| > \delta_{macro}$  { $k++$ } do
5:       loop over all macro Gauss points
6:         compute macro strain  $\mathbf{E} = \langle \boldsymbol{\varepsilon} \rangle$ ;
7:         compute macro stress  $\boldsymbol{\Sigma} = \langle \boldsymbol{\sigma} \rangle$  (see Algorithm 2);
8:       end loop
9:       update macro solution:  $\mathbf{K}_T \Delta \mathbf{u} = \mathbf{f}_{ext} - \int_{\Omega} \mathbf{B}^T \langle \boldsymbol{\sigma} \rangle d\Omega$ ;
10:      end while
11:    end loop
12:    compute the objective  $c(\rho)$  and velocity  $v_n$ ;
13:    update the level-set  $\psi(x, t)$  and the topology  $\rho(\psi)$ ;
14:  end while
15: return the final design topology  $\rho(\psi)$ .

```

where $\mathbf{K}_T = -\partial \mathbf{R} / \partial \mathbf{u}$ is the tangent stiffness matrix at the converged solution of \mathbf{u} . For accurately evaluating the sensitivity, the perturbation method as presented in Section 2.3 could be used for the determination of \mathbf{K}_T at the convergence. Eq. (23) can be reformulated by regrouping the terms with $\partial \mathbf{u} / \partial \rho_e$

$$\frac{\partial c^*}{\partial \rho_e} = \left(\mathbf{f}_{ext}^T - \mathbf{w}^T \mathbf{K}_T \right) \frac{\partial \mathbf{u}}{\partial \rho_e} + \mathbf{w}^T \frac{\partial \mathbf{R}}{\partial \rho_e}. \quad (24)$$

In order to eliminate the first term of the Right Hand Side (RHS), we solve

$$\mathbf{K}_T \mathbf{w} = \mathbf{f}_{ext} \quad (25)$$

yielding

$$\frac{\partial c^*}{\partial \rho_e} = \mathbf{w}^T \frac{\partial \mathbf{R}}{\partial \rho_e}, \quad (26)$$

where according to Eq. (17),

$$\frac{\partial \mathbf{R}}{\partial \rho_e} = - \int_{\Omega_e} \mathbf{B}^T \langle \boldsymbol{\sigma}(\mathbf{x}, \mathbf{y}) \rangle d\Omega_e. \quad (27)$$

Finally, substituting Eqs. (26) and (27) into Eq. (20), the normal velocity v_n within an element e at the k th design iteration can be determined through

$$v_n|_e = \mathbf{w}_e^T \int_{\Omega_e} \mathbf{B}^T \langle \boldsymbol{\sigma}(\mathbf{x}, \mathbf{y}) \rangle d\Omega_e - \lambda^k - \frac{1}{A^k} (V(\rho) - V_{req}), \quad (28)$$

where \mathbf{w}_e is the corresponding value of \mathbf{w} for element e .

3.3. General design framework

A general optimization framework using the discrete level-set model in coupling with FE² is outlined in Algorithm 1. Generally speaking, there exist three layers in this framework. The very outer layer is the optimization which loops until the design solution has reached convergence. The middle and inner layers are the nested macroscopic and microscopic boundary value problems, i.e., FE². As presented in the previous section, FE² itself is an extremely expensive approach in computation. Here such an expensive approach is embedded in an optimization loop where the computational cost is no longer tolerable. However, this multiscale design problem perfectly suits the ROM learning process due to the loops of similar or even repeated computations of the RVE. A surrogate model based on bi-level model reduction is introduced in the next section to replace full FEA in microscopic analysis.

4. Surrogate model based on bi-level model reduction

The bi-level reduced surrogate model is constructed coupling the POD and Diffuse Approximation procedures. The first level of reduction is achieved by Proper Orthogonal Decomposition (POD), allowing to expand a displacement field as a linear combination of the truncated modes. Secondly, the surrogate model based on Diffuse Approximation is built to express the POD projection coefficients as functions of the average micro strain tensors. Similar treatment has been used in [42] for multidisciplinary optimization of the wing.

4.1. Proper Orthogonal Decomposition of RVE displacement field

We consider a D -dimensional ($D = 2$ or 3) RVE of N points subjected to a time-dependent loading $\mathbf{E}(t) = \langle \boldsymbol{\varepsilon} \rangle(t)$ during a time interval $I = [0, T]$ discretized by M instants $\{t_1, t_2, \dots, t_M\}$. Let $\mathbf{u}_i \in \mathbb{R}^{DN}$ denote the DN -dimensional nodal displacement vector recorded at the instant $t_i \in I$.

The reduced order displacement vector $\mathbf{u}^R(t) \in \mathbb{R}^{DN}$ may be written

$$\mathbf{u}^R(t) = \bar{\mathbf{u}} + \sum_{i=1}^m \boldsymbol{\phi}_i \alpha_i(\langle \boldsymbol{\varepsilon} \rangle(t)), \quad (29)$$

where $m \ll \min(M, DN)$, $\bar{\mathbf{u}} = 1/M \sum_{i=1}^M \mathbf{u}_i$ is the average displacement, $\boldsymbol{\phi}_i \in \mathbb{R}^{DN}$ are constant vectors and coefficients $\alpha_i(\langle \boldsymbol{\varepsilon} \rangle(t))$ are scalar functions of pseudo-time t . $\boldsymbol{\phi}_i$ are the eigenvectors of the eigenvalue problem

$$\mathbf{C}_u \boldsymbol{\phi}_i = \lambda_i \boldsymbol{\phi}_i, \quad (30)$$

where \mathbf{C}_u is the covariance matrix

$$\mathbf{C}_u = \mathbf{D}_u \mathbf{D}_u^T, \quad (31)$$

where \mathbf{D}_u is the deviation matrix of dimensionality $DN \times M$ with centered nodal displacement vectors as columns

$$\mathbf{D}_u = \{\mathbf{u}_1 - \bar{\mathbf{u}}, \dots, \mathbf{u}_M - \bar{\mathbf{u}}\}. \quad (32)$$

The size of the truncated basis m is chosen in consideration of the projection error ϵ induced by the POD procedure

$$\epsilon = 1 - \frac{\sum_{i=1}^m \lambda_i}{\sum_{j=1}^M \lambda_j} < \delta, \quad (33)$$

where δ is a prescribed tolerance.

4.2. Diffuse Approximation of the projection coefficients

The surrogate model of the projection coefficients α_i , $i = 1, \dots, m$, with respect to average stain $\langle \boldsymbol{\varepsilon} \rangle$ in Eq. (29) is constructed using the method of Diffuse Approximation [43]

$$\tilde{\alpha}(\langle \boldsymbol{\varepsilon} \rangle) = \mathbf{p}^T \mathbf{a}, \quad (34)$$

where $\mathbf{p} = [p_1, p_2, \dots]^T$ is the polynomial basis vector. In 2D case, the polynomial basis vector expressed in terms of the average strain in 2D case is

$$\mathbf{p} = [1, \langle \boldsymbol{\varepsilon} \rangle_{11}, \langle \boldsymbol{\varepsilon} \rangle_{22}, \langle \boldsymbol{\varepsilon} \rangle_{12}, \dots]^T. \quad (35)$$

The vector of coefficients $\mathbf{a} = [a_1, a_2, \dots]^T$ is the minimizer of functional defined by

$$J(\mathbf{a}) = \frac{1}{2} \sum_{k=1}^M w_k \left(\mathbf{p}^T \mathbf{a} - \alpha(\langle \boldsymbol{\varepsilon} \rangle_k) \right)^2, \quad (36)$$

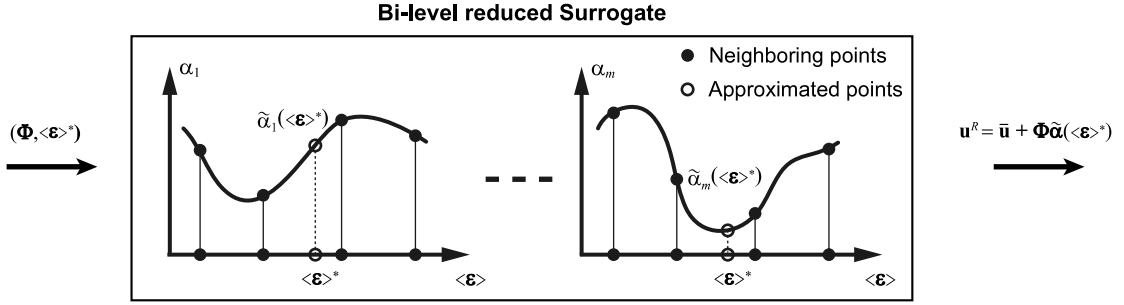


Fig. 5. Illustration of the approximation procedure of the surrogate model.

in which w_k are the weights depending on the Euclidean distance between $\langle \boldsymbol{\varepsilon} \rangle$ and $\langle \boldsymbol{\varepsilon} \rangle_k$

$$w_k = w_{ref} \left(\frac{dist(\langle \boldsymbol{\varepsilon} \rangle, \langle \boldsymbol{\varepsilon} \rangle_k)}{r} \right), \quad (37)$$

where r is a radius defining the local influence zone. w_{ref} is chosen here as a piecewise cubic spline expressed as [44]

$$w_{ref}(s) = \begin{cases} 1 - 3s^2 + 2s^3 & \text{if } 0 \leq s \leq 1 \\ 0 & \text{if } s \geq 1. \end{cases} \quad (38)$$

4.3. Bi-level model reduction

An illustrative flowchart of the approximation procedure is given in Fig. 5. With a given admissible value of average micro strain $\langle \boldsymbol{\varepsilon} \rangle^*$, the corresponding approximated POD projection coefficients from $\tilde{\alpha}_1$ to $\tilde{\alpha}_m$ are locally interpolated using Diffuse Approximation. Thereafter, we have the reduced order solution of the displacement field

$$\mathbf{u}(\langle \boldsymbol{\varepsilon} \rangle^*) \approx \mathbf{u}^R(\langle \boldsymbol{\varepsilon} \rangle^*) \approx \bar{\mathbf{u}} + \Phi\tilde{\boldsymbol{\alpha}}(\langle \boldsymbol{\varepsilon} \rangle^*), \quad (39)$$

where $\Phi = \{\phi_1, \dots, \phi_m\}$ is the reduced basis obtained through POD of RVE displacement fields.

4.4. Application of the surrogate model

The surrogate model is applied to replace full FEA in microscopic analysis. Detailed solution of the microscopic problem is given in Algorithm 2. Computations during the first time step of the first optimization iteration are performed using full FEA to initialize the surrogate model. The surrogate model is then used to replace full FEA in solving the micro problem in the following computations when there are enough neighboring points to perform the approximation. $I(\langle \boldsymbol{\varepsilon} \rangle, \langle \boldsymbol{\varepsilon} \rangle_k)$ in Algorithm 2 is a counting function

$$I(\langle \boldsymbol{\varepsilon} \rangle, \langle \boldsymbol{\varepsilon} \rangle_k) = \begin{cases} 1 & \text{if } dist(\langle \boldsymbol{\varepsilon} \rangle, \langle \boldsymbol{\varepsilon} \rangle_k) \leq r \\ 0 & \text{if } dist(\langle \boldsymbol{\varepsilon} \rangle, \langle \boldsymbol{\varepsilon} \rangle_k) > r, \end{cases} \quad (40)$$

which counts the number of points within the local influence zone r

$$r = \frac{dist((\varepsilon_{11}^{\max}, \varepsilon_{22}^{\max}, \varepsilon_{12}^{\max}), (\varepsilon_{11}^{\min}, \varepsilon_{22}^{\min}, \varepsilon_{12}^{\min}))}{N_{ratio}}, \quad (41)$$

defined as a ratio N_{ratio} of the Euclidean distance between the maximum and minimum strain components in the surrogate. N_{approx} is the required number which is given in accordance with the surrogate size and also the order of the polynomial applied.

When there is no enough points within the local influence zone, the micro problem is solved using full FEA and the results are used to update the POD basis Φ and enrich the surrogate. In this work, the scale of the surrogate is kept constant after its initialization which means the enrichment includes current analysis results while excludes the same number of previous results. At one hand, the previous results no longer contribute in the following designs

Algorithm 2 Solution of the microscopic problem.

- 1: Given $\langle \boldsymbol{\varepsilon} \rangle, i, j, k$;
- 2: Define boundary conditions on RVE upon $\langle \boldsymbol{\varepsilon} \rangle$ using Eq. (6);
- 3: **if** $i = 1$ and $j = 1$ **then**
- 4: compute $\langle \boldsymbol{\sigma} \rangle$ using full FEA (Eq. (7));
- 5: extract the POD basis Φ and construct the surrogate;
- 6: **else if** $\sum_k I(\langle \boldsymbol{\varepsilon} \rangle, \langle \boldsymbol{\varepsilon} \rangle_k) < N_{approx}$ or $k \geq N_{sub}$ **then**
- 7: compute $\langle \boldsymbol{\sigma} \rangle$ using full FEA;
- 8: update the POD basis Φ and enrich the surrogate;
- 9: **else**
- 10: compute $\langle \boldsymbol{\sigma} \rangle$ using the surrogate: $\mathbf{u} \approx \bar{\mathbf{u}} + \Phi \tilde{\boldsymbol{\alpha}}(\langle \boldsymbol{\varepsilon} \rangle)$;
- 11: **end if**
- 12: **return** the micro average stress $\langle \boldsymbol{\sigma} \rangle$.

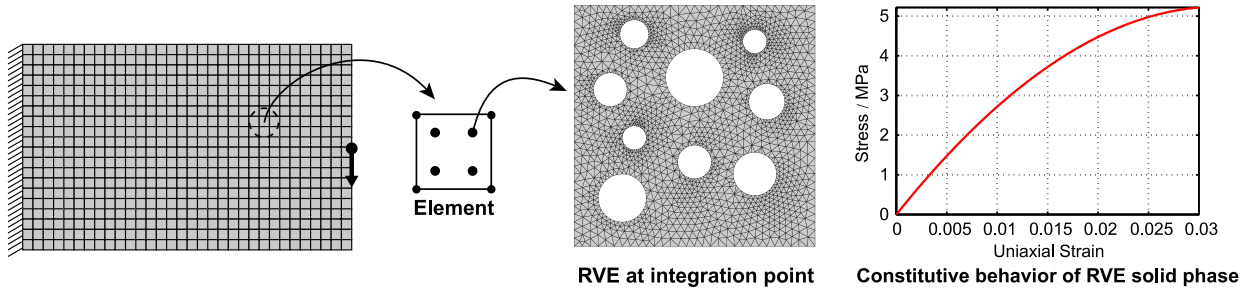


Fig. 6. Illustration of the test example.

as the structural topology varies; at another hand, the Diffuse Approximation becomes more and more expensive in computing as the surrogate scale grows.

In case when the macroscopic convergence in Algorithm 1 cannot be reached after a certain number of substeps, i.e., $\|\mathbf{f}_{ext} - \mathbf{f}_{int}\| > \delta_{macro}$, we can either shrink local influence zone r , or force to use full FEA to update the surrogate model. The latter solution is recommended in consideration of both aspects of analysis accuracy and the efficiency in convergence. In this algorithm, full FEA is applied to perform microscopic computing after a certain number of macroscopic substeps, i.e., $k \geq N_{sub}$.

5. Numerical examples

The benchmark cantilever problem [29] is considered in this section with anisotropic material defined at the microscopic scale. As illustrated in Fig. 6, the macroscopic structure is discretized into 32×20 four-node plane strain elements where each element has four Gauss integration points. Each Gauss point in the macroscopic structure corresponds to a considered RVE in the microscopic scale. The material property of the solid phase in the RVE is assumed to be isotropic with a nonlinear elastic constitutive behavior as shown in Fig. 6. Conventional unreduced FE² approach requires $32 \times 20 \times 4$ independent RVE analyses at the microscopic scale for one time evaluation at the macroscopic scale. For the sake of simplicity, the initial elastic stiffness matrix have been kept during the Newton–Raphson iterative resolution procedure. In order to perform sensitivity analysis, tangent stiffness matrix is evaluated using the perturbation method at the converged moment of each design iteration.

5.1. Test case 1

In the first test case, the value of the external loading force is set to 0.5 N and the considered volume constraint is 40%. The parameters in Eq. (19) is set as $\alpha = 0.9$, $\lambda = -10^{-8}$, $\Lambda = 4 \times 10^7$. The tolerance error in Eq. (33) is set as $\delta = 10^{-6}$. The extracted POD modes vary adaptively during the optimization procedure and the size of the reduced basis is 5 and stays constant. In Fig. 7, we show the resultant tractions, used in Eq. (7) of the first 5 final POD modes along with the associated normalized eigenvalues λ_i/λ_{max} . The ratio in Eq. (41) to define the influence zone is set as $N_{ratio} = 20$, and the required number of approximating points in Algorithm 2 is set as $N_{approx} = 7$.

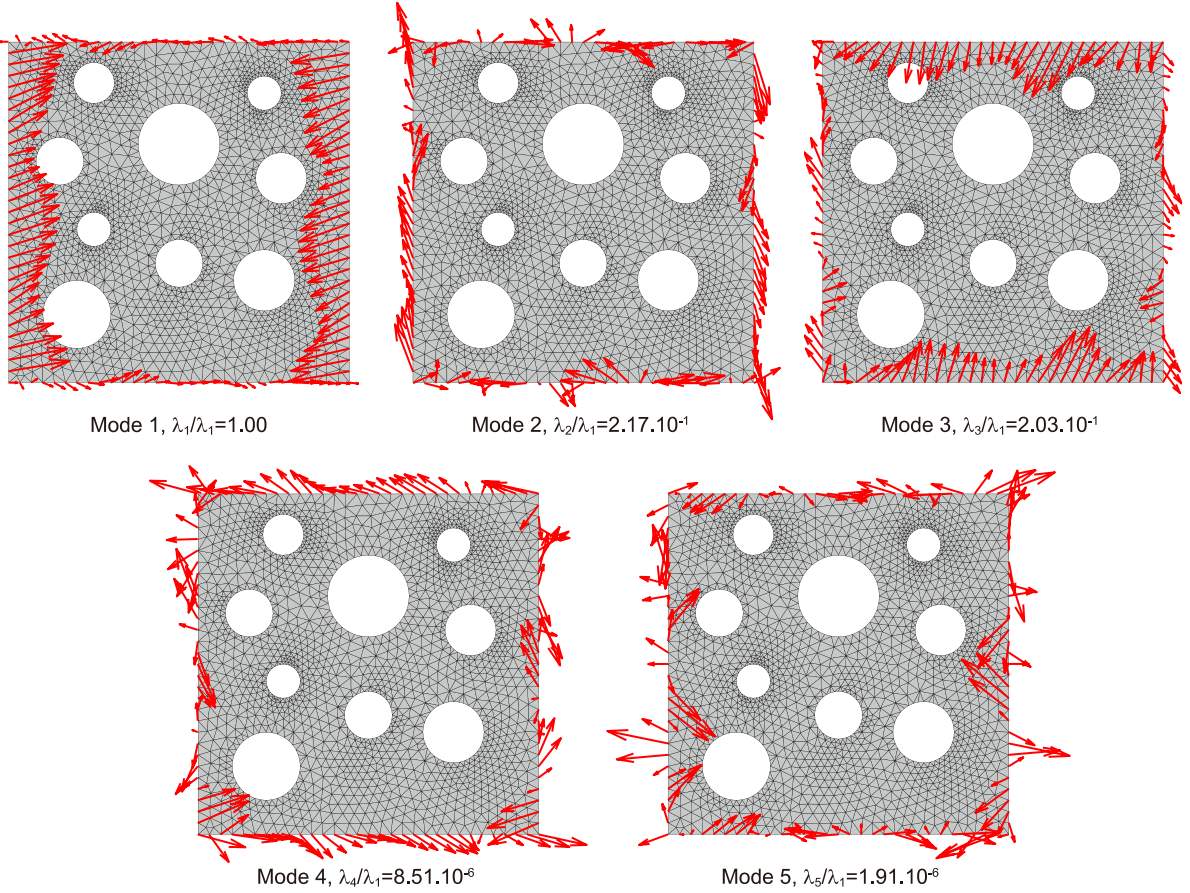


Fig. 7. Resultant tractions of the first 5 POD modes after the optimization.

The structural topological evolution in the macroscopic scale is given in Fig. 8. Usually topology optimization gives a symmetric design result when isotropic material constitutive behavior is considered due to the symmetry of the cantilever problem. However, the final structural design obtained here is no longer symmetric due to the anisotropy of the considered RVE at the microscopic scale. The convergence histories of the strain energy and the volume ratio are demonstrated in Fig. 9(a) and (b), respectively.

During the loading phase of the first optimization iteration, the periodic homogenizations of the RVE at the microscopic scale are performed using full FEA. Since the second optimization iteration, both FEA and the surrogate model are used for the microscopic analyses. Fig. 9(c) gives the percentage of FEA usage in each optimization iteration. It can be seen that less than 4% microscopic analyses require using full FEA due to the usage of surrogate model, which significantly reduces computational cost. The jumps in Fig. 9(c) correspond to comparatively large volume and topological variations which require more usage of FEA in order to update the POD basis and enrich the surrogate model.

The same optimization design has also been performed without using the surrogate. The unreduced FE² approach gives an exactly the same optimization design result as the reduced model where the relative errors of the objective are less than 10^{-5} . The iterative computing time using the unreduced FE² decreases as the volume ratio decreases (see Fig. 9(b)), i.e., the number of micro analysis required in each substep of macroscopic computing decreases from the maximum $0.8 \times 32 \times 20 \times 4$ to finally $0.4 \times 32 \times 20 \times 4$. Generally speaking, it requires around two hours of computing for each optimization iteration on a HP Z420 Workstation when using the unreduced sequential FE². In contrast, the reduced FE² approach requires only ten minutes of computing on average for each design iteration apart from the first design iteration. More savings in computation can be expected using the reduced approach when larger scale problems are considered.

Fig. 10 depicts the equivalent strain distributions at the microscopic scale at selected points. One may note that the existence of the holes in the RVE concentrates much higher strains and hence stresses in the microscopic scale than the

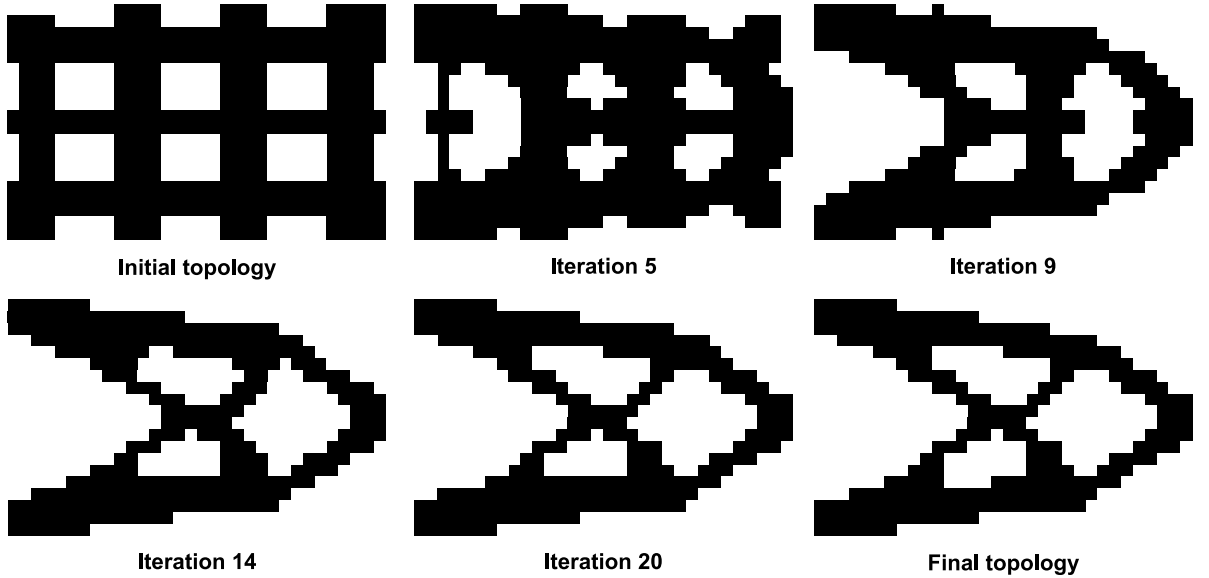


Fig. 8. Structural topology variations during the optimization process.

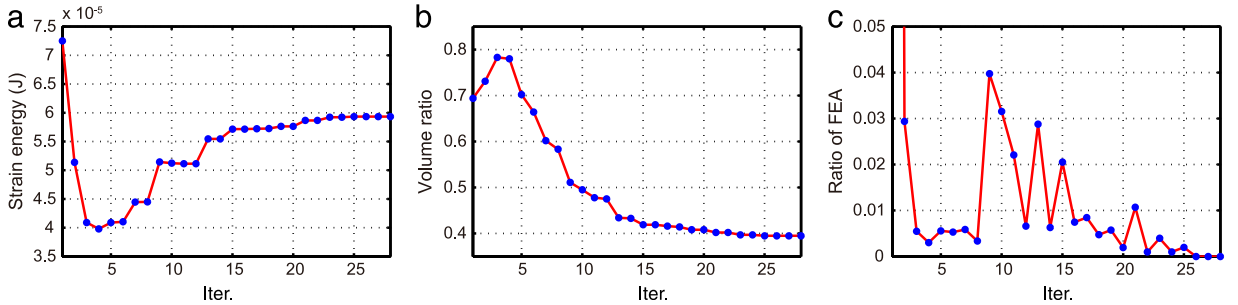


Fig. 9. Optimization history: (a) convergence history of the strain energy, (b) convergence history of the volume ratio, (c) the ratio of FEA usage in each iteration.

homogenized macroscopic values. Moreover, different micro strain distributions manifest the difference of the local loading statuses of the selected points, where point c in the center of the structure obviously suffers more mechanical loads than typical points (a, b, d) located off the main loading region. The higher stress concentration may lead to the initial material failure or crack at the micro scale which cannot be detected when using the conventional one scale fracture analysis [45]. There is also a potential application of such feature in stress-related topological designs [46, 47], where the stress constraints may be considered to limit the maximum stress at the micro scale.

5.2. Test case 2

In order to evaluate the performance of the surrogate model when encountering more nonlinearity and more severe topological changes, the external loading force is increased to 1.5 N and the considered volume ratio constraint is decreased to 32%. The parameters in Eq. (19) is set as $\alpha = 0.9$, $\lambda = -10^{-7}$, $\Lambda = 7 \times 10^6$. The tolerance error in Eq. (33) is set as in the previous case of $\delta = 10^{-6}$. Correspondingly, the number of retained POD modes increases to 6 during the first iterations and then to 7 during the following iterations until the end. The resultant tractions of the first 7 of the final POD modes are shown in Fig. 11 together with their associated normalized eigenvalues λ_i/λ_{\max} . The ratio in Eq. (41) to define the influence zone is set as $N_{ratio} = 20$, and the required number of approximating points in Algorithm 2 is set as $N_{approx} = 7$.

The structural topological evolution in the macroscopic scale given in Fig. 12 is similar to the previous case during the first iterations while differs later due the applied lower volume ratio constraint. The convergence histories of the strain energy and of the volume ratio are demonstrated in Fig. 9(a) and (b), respectively.

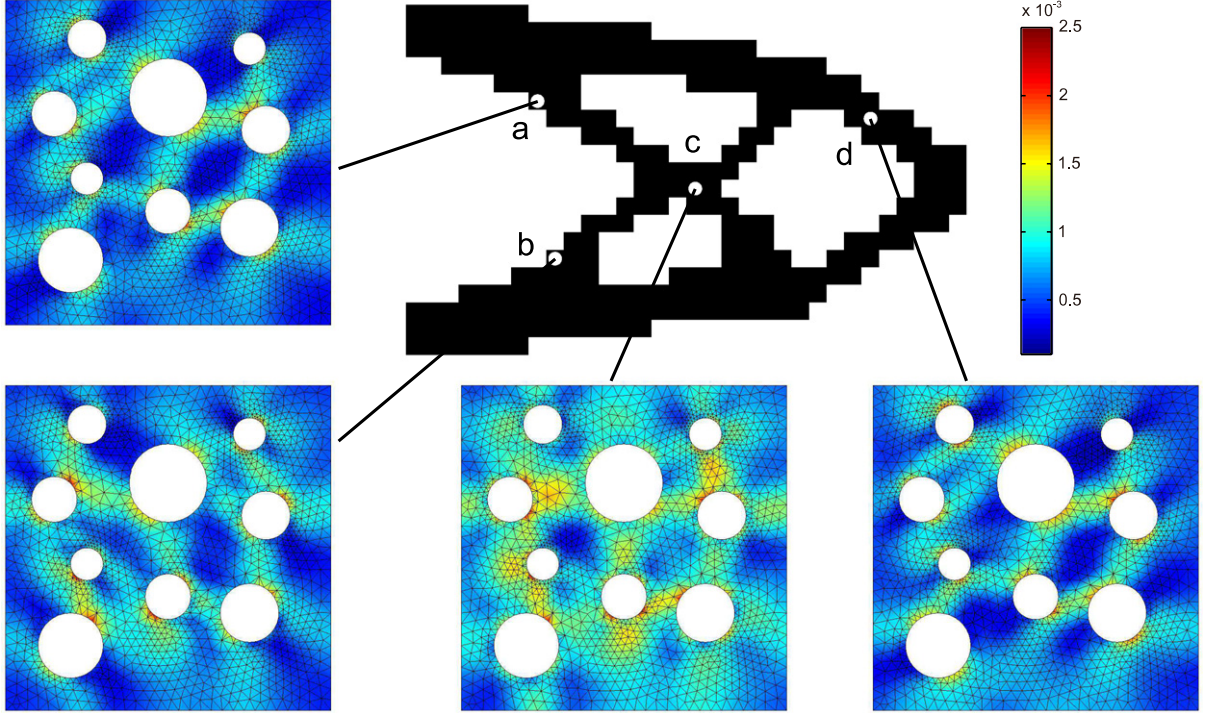


Fig. 10. Microscopic scale equivalent strain distributions at selected points.

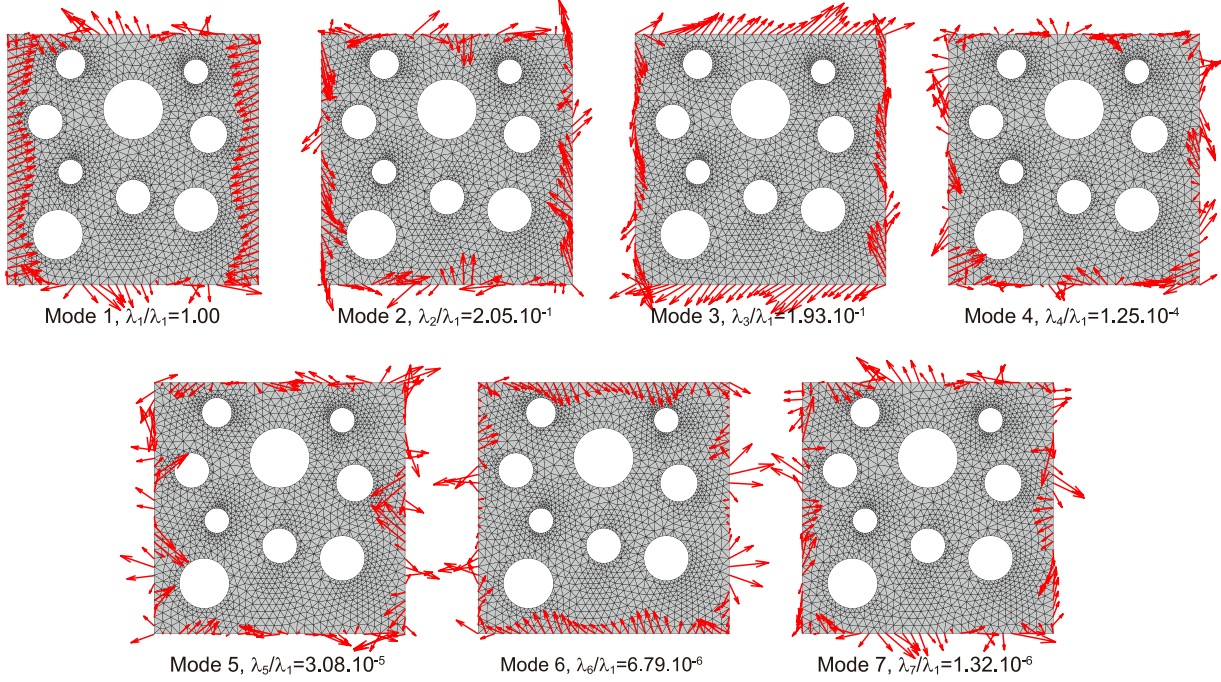


Fig. 11. Resultant tractions of the first 7 POD modes after the optimization.

Likewise, the surrogate model is initialized during the loading phase of the first optimization iteration. Both the surrogate model and FEA are used in the following optimization iterations. Fig. 13(c) gives the percentage of FEA usage in each optimization iteration. Similar to the previous case, less than 4% microscopic analyses require using

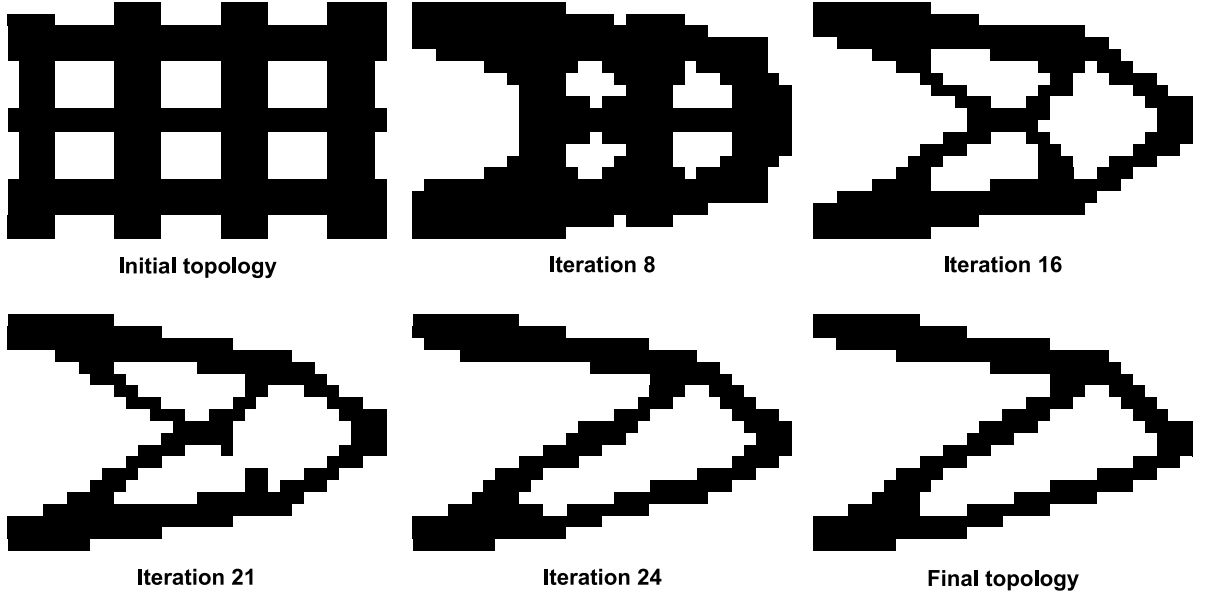


Fig. 12. Structural topology variations during the optimization process.

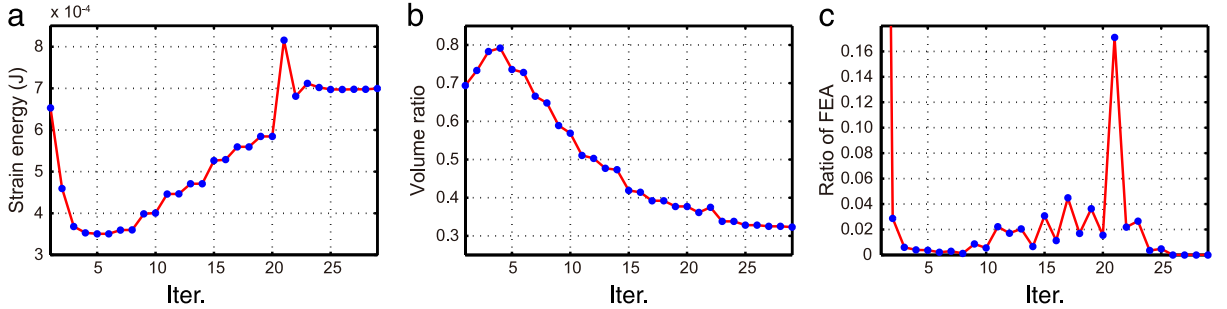


Fig. 13. Optimization history: (a) convergence history of the strain energy, (b) convergence history of the volume ratio, (c) the ratio of FEA usage in each iteration.

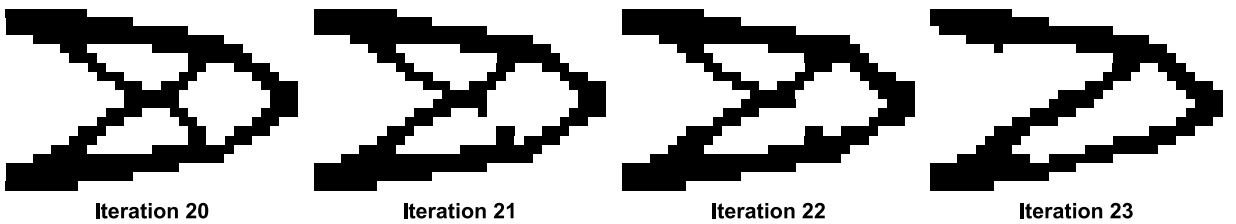


Fig. 14. Intermediate design topologies from iteration 20 to iteration 23.

full FEA except a jump from 2% in iteration 20 to 17% in iteration 21. A detailed illustration of the topological evolution around iteration 21 is given in Fig. 14. It can be seen that a branch of the structure splits in iteration 21. Such a severe topological variation results in a large variation of the structural physical response and hence the surrogate built according to the previous calculations is no longer accurate enough. Therefore, an increased number of full FEA is required to recompute the set of the reduced basis. The surrogate model is updated thereafter and the usage ratio of FEA drops back below 4% and decreases to 0% in the following iterations as the structural topology converges, meaning that all computations are performed using the surrogate.

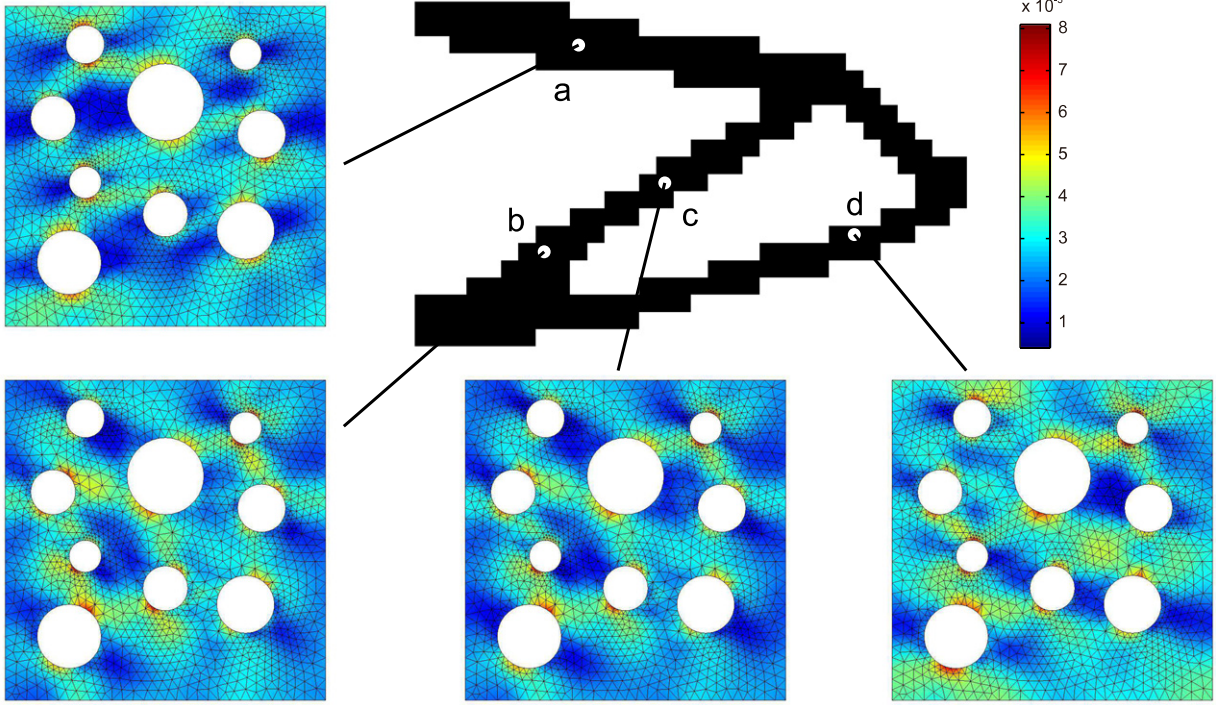


Fig. 15. Microscopic scale equivalent strain distribution at selected points.

For the purpose of comparison, the same optimization design has also been performed using the unreduced FE² approach which gives exactly the same optimization design result as obtained above where the relative errors of the objective for each design iteration are less than 10^{-5} . As shown in Fig. 13(b), the number of micro analyses required in each substep of macroscopic computing varies from the maximum $0.8 \times 32 \times 20 \times 4$ to finally $0.32 \times 32 \times 20 \times 4$. Due to the increased nonlinearity, more substeps have to be taken to reach the macro convergence and thereafter the average computing time for each optimization augments to around three hours. Similarly, more substeps are required to reach the macro convergence when using the surrogate and average computing time required by the reduced approach increases to fifteen minutes, which is nevertheless a significant gain in time compared to the time required using the unreduced approach.

Fig. 15 depicts the equivalent strain distributions at the microscopic scale at selected points. Because of the increase of the external loading force and the decrease of the volume ratio constraint, larger deformations can be observed from the equivalent strain distributions at the microscopic scale. The micro strain distributions clearly manifest the difference of the loading status in different structural branches. The micro strain distributions at points b and c are quite similar because they are located in the same branch of the structure.

6. Conclusion and perspectives

In this work, we have proposed a reduced multiscale model for macroscopic structural design considering microscopic material nonlinear microstructures. Several established techniques have been applied: the structural design is realized using a discrete level-set topology optimization model, the multiscale analysis is performed using the FE² approach, and the surrogate model is constructed using POD and Diffuse Approximation. The surrogate model is constructed in an on-line manner: initially built during the first optimization design iteration is then updated in the following design iterations. It has been observed that the surrogate model can significantly reduce the computational cost, particularly when multiple loops involving similar computations are required.

Further improvement of the proposed model could be the employment of the advanced models of any of the applied techniques, such as considering nucleation in level-set topology optimization in order to avoid an artificially defined

initial topology, considering the size effect in multiscale analysis, and other possible strategies to perform model reduction either in an intrusive manner or non-intrusive manner using different approaches to construct the surrogate.

In the present work, as a first step towards FE²-based nonlinear structural design, only nonlinear elasticity with the infinitesimal strain is considered at the microscopic scale. For this simple case, it could be an easier solution to build an interpolating relationship directly between the stress and strain at the microscopic scale which may perform well. The present algorithm using the field interpolation is more accurate and the on-line learning procedure is more suitable for capturing nonlinear features. Moreover, the undergoing developments intend to handle more complex nonlinear cases, where an on-line learning process is highly required, for instance path-dependent nonlinearity in elastoplastic analysis.

Based on the proposed work, our future works will be focused on improving macroscopic structural mechanical performance through the optimization design of the RVE microstructure with respect to geometrical or manufacturing process parameters. FE² approach has a great advantage to perform such kind of microscopic optimization, because the optimized microstructures can be homogenized in a concurrent manner when performing multiscale analysis. Nevertheless, the problem becomes more computational time-consuming due the larger number of sub-optimization designs. In such case, off-line reduction approaches could be possible solutions to reduce the extremely high computing demand.

Acknowledgments

This work was carried out in the framework of the Labex MS2T, which was funded by the French Government, through the program “Investments for the future” managed by the National Agency for Research (Reference ANR-11-IDEX-0004-02). This work is also funded by the China Scholarship Council (CSC).

References

- [1] D.T. Fullwood, S.R. Niezgoda, B.L. Adams, S.R. Kalidindi, Microstructure sensitive design for performance optimization, *Prog. Mater. Sci.* 55 (6) (2010) 477–562.
- [2] R.J.M. Smit, W.A.M. Brekelmans, H.E.H. Meijer, Prediction of the mechanical behavior of nonlinear heterogeneous systems by multi-level finite element modeling, *Comput. Methods Appl. Mech. Engrg.* 155 (1–2) (1998) 181–192.
- [3] C. Miehe, J. Schröder, J. Schotte, Computational homogenization analysis in finite plasticity simulation of texture development in polycrystalline materials, *Comput. Methods Appl. Mech. Engrg.* 171 (3–4) (1999) 387–418.
- [4] F. Feyel, J. Chaboche, FE² multiscale approach for modelling the elastoviscoplastic behaviour of long fibre Sic/Ti composite materials, *Comput. Methods Appl. Mech. Engrg.* 183 (3–4) (2000) 309–330.
- [5] V. Kouznetsova, W.A.M. Brekelmans, F.P.T. Baaijens, An approach to micro–macro modeling of heterogeneous materials, *Comput. Mech.* 27 (1) (2001) 37–48.
- [6] S. Ghosh, K. Lee, P. Raghavan, A multi-level computational model for multi-scale damage analysis in composite and porous materials, *Internat. J. Solids Structures* 38 (14) (2001) 2335–2385.
- [7] A. Ibrahimbegovic, D. Markovic, Strong coupling methods in multi-phase and multi-scale modeling of inelastic behavior of heterogeneous structures, *Comput. Methods Appl. Mech. Engrg.* 192 (28–30) (2003) 3089–3107.
- [8] A. Ibrahimbegovic, M. Papadrakakis, Multi-scale models and mathematical aspects in solid and fluid mechanics, *Comput. Methods Appl. Mech. Engrg.* 199 (21–22) (2010) 1241.
- [9] M.G.D. Geers, V.G. Kouznetsova, W.A.M. Brekelmans, Multi-scale computational homogenization: trends and challenges, *J. Comput. Appl. Math.* 234 (7) (2010) 2175–2182.
- [10] N.B. Queipo, R.T. Haftka, W. Shyy, T. Goel, R. Vaidyanathan, P.K. Tucker, Surrogate-based analysis and optimization, *Prog. Aerosp. Sci.* 41 (1) (2005) 1–28.
- [11] A. Forrester, A. Keane, Recent advances in surrogate-based optimization, *Prog. Aerosp. Sci.* 45 (1–3) (2009) 50–79.
- [12] A. Ammar, B. Mokdad, F. Chinesta, R. Keunings, A new family of solvers for some classes of multidimensional partial differential equations encountered in kinetic theory modeling of complex fluids, *J. Non-Newton. Fluid Mech.* 139 (3) (2006) 153–176.
- [13] D. Ryckelynck, A priori hyperreduction method: an adaptive approach, *J. Comput. Phys.* 202 (1) (2005) 346–366.
- [14] D. Ryckelynck, F. Vincent, S. Cantournet, Multidimensional a priori hyper-reduction of mechanical models involving internal variables, *Comput. Methods Appl. Mech. Engrg.* 225–228 (2012) 28–43.
- [15] F. Fritzen, T. Böhlke, Three-dimensional finite element implementation of the nonuniform transformation field analysis, *Internat. J. Numer. Methods Engrg.* 84 (7) (2010) 803–829.
- [16] F. Fritzen, T. Böhlke, Nonuniform transformation field analysis of materials with morphological anisotropy, *Compos. Sci. Technol.* 71 (4) (2011) 433–442.
- [17] B. Ganapathysubramanian, N. Zabaras, Modeling diffusion in random heterogeneous media: data-driven models, stochastic collocation and the variational multiscale method, *J. Comput. Phys.* 226 (1) (2007) 326–353.

- [18] L. Xia, B. Raghavan, P. Breitkopf, W. Zhang, Numerical material representation using proper orthogonal decomposition and diffuse approximation, *Appl. Math. Comput.* 224 (2013) 450–462.
- [19] M. Xiao, P. Breitkopf, R. Filomeno Coelho, C. Knopf-Lenoir, M. Sidorkiewicz, P. Villon, Model reduction by CPOD and Kriging: application to the shape optimization of an intake port, *Struct. Multidiscip. Optim.* 41 (4) (2010) 555–574.
- [20] B. Raghavan, L. Xia, P. Breitkopf, A. Rassineux, P. Villon, Towards simultaneous reduction of both input and output spaces for interactive simulation-based structural design, *Comput. Methods Appl. Mech. Engrg.* 265 (1) (2013) 174–185.
- [21] J. Yvonnet, Q.C. He, The reduced model multiscale method (R3M) for the non-linear homogenization of hyperelastic media at finite strains, *J. Comput. Phys.* 223 (1) (2007) 341–368.
- [22] F. El Halabi, D. González, A. Chico, M. Doblaré, Fe2 multiscale in linear elasticity based on parametrized microscale models using proper generalized decomposition, *Comput. Methods Appl. Mech. Engrg.* 257 (2013) 183–202.
- [23] M. Cremonesi, D. Nérón, P. Guidault, P. Ladenvèze, A PGD-based homogenization technique for the resolution of nonlinear multiscale problems, *Comput. Methods Appl. Mech. Engrg.* 267 (2013) 275–292.
- [24] J.D. Deaton, R.V. Grandhi, A survey of structural and multidisciplinary continuum topology optimization: post 2000, *Struct. Multidiscip. Optim.* 49 (1) (2014) 1–38.
- [25] M.P. Bendsøe, N. Kikuchi, Generating optimal topologies in structural design using a homogenization method, *Comput. Methods Appl. Mech. Engrg.* 71 (2) (1988) 197–224.
- [26] M.P. Bendsøe, Optimal shape design as a material distribution problem, *Struct. Optim.* 1 (4) (1989) 193–202.
- [27] Y.M. Xie, G.P. Steven, A simple evolutionary procedure for structural optimization, *Comput. Struct.* 49 (5) (1993) 885–896.
- [28] M.Y. Wang, X. Wang, D. Guo, A level set method for structural topology optimization, *Comput. Methods Appl. Mech. Engrg.* 192 (1–2) (2003) 227–246.
- [29] G. Allaire, F. Jouve, A.M. Toader, Structural optimization using sensitivity analysis and a level-set method, *J. Comput. Phys.* 194 (1) (2004) 363–393.
- [30] O. Sigmund, K. Maute, Topology optimization approaches—a comparative review, *Struct. Multidiscip. Optim.* 48 (6) (2013) 1031–1055.
- [31] P.B. Nakshatrala, D.A. Tortorelli, K.B. Nakshatrala, Nonlinear structural design using multiscale topology optimization. Part i: static formulation, *Comput. Methods Appl. Mech. Engrg.* 261–262 (2013) 167–176.
- [32] V.J. Challis, A discrete level-set topology optimization code written in matlab, *Struct. Multidiscip. Optim.* 41 (3) (2010) 453–464.
- [33] B. Nayroles, G. Touzot, P. Villon, Generalizing the finite element method: diffuse approximation and diffuse elements, *Comput. Mech.* 10 (5) (1992) 307–318.
- [34] P. Lancaster, K. Salkauskas, Surfaces generated by moving least squares methods, *Math. Comp.* 87 (1981) 141–158.
- [35] J. Guedes, N. Kikuchi, Preprocessing and postprocessing for materials based on the homogenization method with adaptive finite element methods, *Comput. Methods Appl. Mech. Engrg.* 83 (2) (1990) 143–198.
- [36] J.C. Michel, H. Moulinec, P. Suquet, Effective properties of composite materials with periodic microstructure: a computational approach, *Comput. Methods Appl. Mech. Engrg.* 172 (1–4) (1999) 109–143.
- [37] Z. Xia, Y. Zhang, F. Ellyin, A unified periodical boundary conditions for representative volume elements of composites and applications, *Internat. J. Solids Structures* 40 (8) (2003) 1907–1921.
- [38] Z. Xia, C. Zhou, Q. Yong, X. Wang, On selection of repeated unit cell model and application of unified periodic boundary conditions in micro-mechanical analysis of composites, *Internat. J. Solids Structures* 43 (2) (2006) 266–278.
- [39] M. Burger, B. Hackl, W. Ring, Incorporating topological derivatives into level set methods, *J. Comput. Phys.* 194 (1) (2004) 344–362.
- [40] T. Belytschko, S. Xiao, C. Parimi, Topology optimization with implicit functions and regularization, *Internat. J. Numer. Methods Engrg.* 57 (8) (2003) 1177–1196.
- [41] J. Luo, Z. Luo, L. Chen, L. Tong, M.Y. Wang, A semi-implicit level set method for structural shape and topology optimization, *J. Comput. Phys.* 227 (11) (2008) 5561–5581.
- [42] R. Filomeno Coelho, P. Breitkopf, C. Knopf-Lenoir, P. Villon, Bi-level model reduction for coupled problems, *Struct. Multidiscip. Optim.* 39 (4) (2009) 401–418.
- [43] P. Breitkopf, G. Touzot, P. Villon, Consistency approach and diffuse derivation in element free methods based on moving least squares approximation, *Comput. Assist. Mech. Eng. Sci.* 5 (4) (1998) 479–501.
- [44] P. Breitkopf, A. Rassineux, J.M. Savignat, P. Villon, Integration constraint in diffuse element method, *Comput. Methods Appl. Mech. Engrg.* 193 (12–14) (2004) 1203–1220.
- [45] E.W.C. Coenen, V.G. Kouznetsova, M.G.D. Geers, Multi-scale continuous–discontinuous framework for computational-homogenization-localization, *J. Mech. Phys. Solids* 60 (8) (2012) 1486–1507.
- [46] P. Duysinx, M.P. Bendsøe, Topology optimization of continuum structures with local stress constraints, *Internat. J. Numer. Methods Engrg.* 43 (8) (1998) 1453–1478.
- [47] M. Bruggi, P. Duysinx, Topology optimization for minimum weight with compliance and stress constraints, *Struct. Multidiscip. Optim.* 46 (3) (2012) 369–384.